Snihirova, D.; Lamaka, S.V.; Gonzalez-Garcia, Y.; Yilmaz, A.;
Scharnagl, N.; Montemor, M.F.; Zheludkevich, M.L.:
Influence of inhibitor adsorption on readings of microelectrode during SVET measurements.
In: Electrochimica Acta. Vol. 322 (2019) 134761.
First published online by Elsevier: 24.08.2019

https://dx.doi.org/10.1016/j.electacta.2019.134761

Influence of inhibitor adsorption on readings of microelectrode during SVET measurements

D. Snihirova[1,*], S.V. Lamaka[1], Y. Gonzalez-Garcia[2], A. Yilmaz[2], N. Scharnagl[1], M.F. Montemor[3], M.L. Zheludkevich[1,4]

[1]*Institute of Materials Research - Magnesium Innovation Centre MagIC, Helmholtz-Zentrum Geesthacht – Centre for Materials and Coastal Research GmbH, Max-Plank Str.1, 21502 Geesthacht, Germany*
[2]*Department of Materials Science and Engineering, Delft University of Technology, 2628 CD Delft, The Netherlands*
[3]*CQE-Centro de Química Estrutural, DEQ−Departamento de Engenharia Química, Instituto Superior Técnico, Univercity of Lisbon, 1049-001 Lisbon, Portugal*
[4]*Faculty of Engineering, Kiel University, Kaiserstrasse 2, 24143 Kiel, Germany*

[*] Corresponding Author darya.snihirova@hzg.de

Abstract Text

One of the main applications of SVET in corrosion research is the study of the corrosion inhibition effectiveness and the evaluation of the self-healing effect of inhibitor-containing coatings. The tip of the platinum/iridium vibrating electrode is electroplated with black platinum, which creates a large electrode surface and confers high capacitance to the tip. When studying organic inhibitors in aqueous solutions with SVET, inhibitor adsorption may occur at the tip, causing its contamination and the initial calibration conditions of the system might not be valid. This may lead to an incorrect interpretation of the results.

This work is intended to study the effect of different inhibitors (cerium nitrate, 8-hydroxyquinoline, potassium 2,5-dimercapto-1,3,4-thiadiazolate, benzotriazole and mercaptobenzothiazole), typically used for corrosion protection of aluminum alloys, on the Pt probe signal during SVET measurements. The results reveal the detrimental effect of some corrosion inhibitors on the sensitivity of the vibrating probe, an effect that imposes a regular assessment of the electrode state during measurements. The increase of the signal noise was related to a decrease of the probe capacitance, while the false current density signal was a result of the potential drift between vibrating and reference electrodes.

Keywords: SVET; inhibitors; 8-hydroxyquinoline; mercaptobenzothiazole; self-healing

Introduction

Corrosion scientists use a number of different scanning localized electrochemical techniques to resolve local electrochemical phenomena at the microscale level. Among them is the scanning vibrating electrode technique (SVET). It was developed by biologists [1-5], and was adapted to corrosion research purposes by Hugh Isaacs in the 1980s [6-9]. By means of sensitive microelectrodes, the microscale events at the solid/liquid interface are studied for discriminating the mechanisms governing the electrochemical processes.

SVET is a non-destructive technique, with a micron spatial resolution, and has been intensively used to study the performance of corrosion inhibitors [10-20] and to evaluate the self-healing effect of anti-corrosion coatings [21-30]. SVET allows in-situ monitoring of ionic fluxes generated at corrosion sites by means of a vibrating probe (hereafter VP). The current density in solution is calculated as

$$i = -k\frac{\Delta V}{\Delta r} \quad , \tag{1}$$

where i is current density, k is the solution conductivity, ΔV is the potential gradient in the solution measured between two points at distance Δr. In practice, calibration is needed to convert the measured local potential difference into current density values. The spatial resolution of SVET depends on distance between the VP and sample surface, and the magnitude of the currents [31, 32]. Eventually the spatial resolution is limited by the probe tip, typically 5-50 μm [33].

Usually the effect of the inhibitor is evaluated by mapping the current densities over bare metal when it is in contact with a corrosive solution containing the inhibitor. The corrosion inhibitors performance could be assessed by following the changes of current density over an extended period of time [12, 16-20]. Kallip et all. [10] used SVET for high-throughput screening of corrosion inhibitors in multi-material assemblies. This approach allowed evaluating the effect of corrosion inhibitors on different metals and alloys simultaneously. The method is useful when a large number of inhibitors and materials are tested, as in multi-material assemblies [11, 13-15]. Another notable example is to look for a possible synergistic effect of inhibitors in multi-metal cell composed of Al, Cu and Mg, as representative of S-phase intermetallic particles in AA2024 [13]. It was possible to detect the local anodic and cathodic current densities over each metal and to understand the role of individual inhibitors and their mixtures.

SVET is also used for evaluating the self-healing abilities in organic coatings [34, 35] and for monitoring the active corrosion protection in defects of coated samples [21-30]. Changes of the current density over the defect indicated the possible self-healing or smart response of the coating. A comprehensive overview of SVET applications, as well as the basic principles of the technique, can be found in [1-9, 36-38]. SVET possesses good spatial resolution and offers the possibility of detecting low current densities due to the advanced noise reduction. Higher sensitivity and lower

noise are achieved by vibration of the electrode. This creates a sinusoidal signal which is used by lock-in amplifier to rise the signal and reduce noise [1, 36]. However, potential SVET users should be aware of possible limitations in order to avoid certain underestimation of true current, which may lead to a false interpretation of the results. Once the initial conditions used during calibration are changed, the deviation from the measured current density may appear. The first works on SVET in corrosion research already warned users about potential pitfalls of the technique, among which the most insidious are the insufficient capacitance of the VP and the inappropriate shielding and grounding [5]. Recent works discuss the artifacts and limitations of the technique related to the conductivity changes during long-term measurements, and the influence of the probe vibration and movement on SVET results [31, 36, 39-41]. However, the most common problem that can develop during measurement is the loss of the VP capacitance.

This work illustrates the artifacts related to loss of the VP capacitance due to the adsorption of the organic inhibitors to the platinized tip. The tip of the platinum/iridium VP is electroplated with black platinum, which results in a large electrode surface and makes the tip highly capacitive. However, when studying aqueous solutions containing organic corrosion inhibitors by SVET, the inhibitors may interact with the platinum tip causing the VP contamination. As a consequence, the initial calibration is rendered invalid because the measurement conditions have changed, leading to a false interpretation of the results. Literature named possible limitations of SVET caused by the presence of organic inhibitors in aqueous solutions [5]. Contamination of microelectrodes with organic molecules has been noticed when using other localized electrochemical techniques employing Pt probe, like the scanning electrochemical microscopy (SECM) [42]. While studying the effect of MBT on coated AA2024, it was found that the inhibitive species released from the coating were adsorbed on the SECM platinum tip, partially blocking the sensing tip and decreasing the active area of the microelectrode. Artefacts need therefore to be considered when using localized electrochemical techniques with the Pt microelectrodes.

The aim of this work was to study the possible influence of the inhibitors on the reading of the VP in an aqueous solution during SVET tests. The following corrosion inhibitors, which are typically used for the protection of aluminum alloys, were studied: cerium nitrate, 8-hydroxyquinoline, potassium 2,5-dimercapto-1,3,4-thiadiazolate, benzotriazole, mercaptobenzothiazole.

Experimental

Scanning vibrating electrode technique.

Applicable Electronics (MA, USA) instrumentation was used for the measurements. The apparatus uses commercial 80%/20% Pt-Ir micro-electrodes from “MicroProbes for Life Science” (PI

0036.0a10) as VP. The insulated body of the microelectrode had a 10 µm diameter tip, which was plated with black platinum before every measurement. Platinization was conducted from an aqueous solution prepared by mixing 18 mL Millipore water, 2.0 mL of 10% chloroplatinic acid and 0.2 mL of 1% lead acetate. The VP and bare Pt wire were immersed in plating solution. First, a -200nA current was applied to the VP for slow plating during 1 minute. Then, a 2 Hz pulsed current between 0 and -1000nA was applied for 10 seconds. A VP suitable for the measurements should have ca. 2 nF of capacitance [5], although 1nA is still in tolerant range for Applicable Electronics equipment [36].

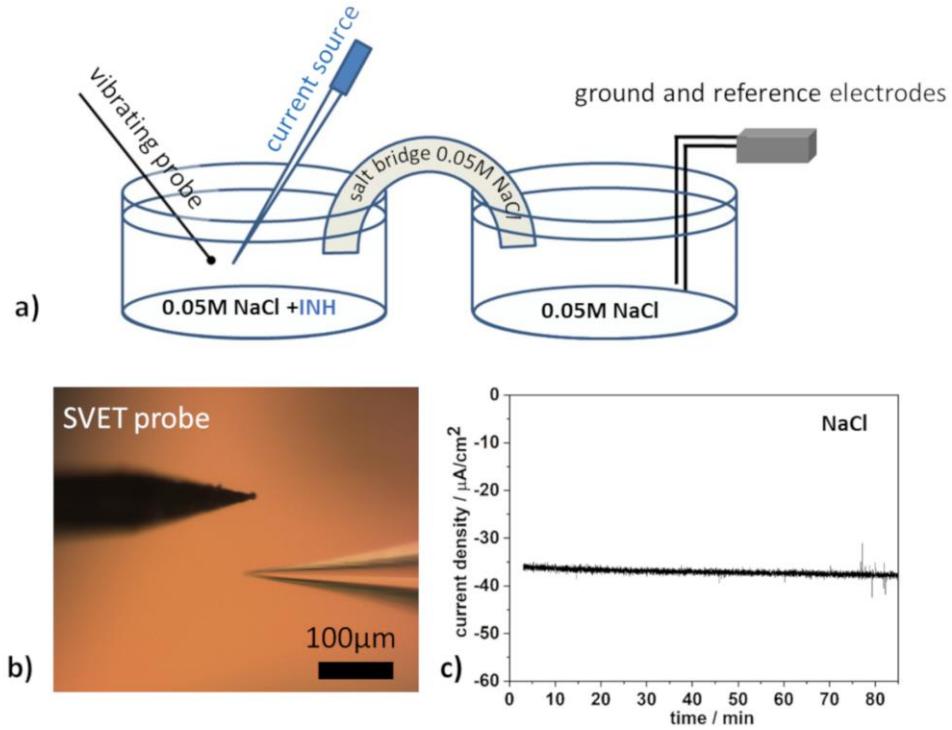

Figure 1. a) Scheme of the experimental setup used during SVET measurements, b) micrograph of the SVET probe and current source, c) signal of the SVET probe in 0.05 M NaCl (supplied current of -60 nA).

The amplitude of VP in the horizontal plane was adjusted manually at a x14 magnification. Vibration in vertical plane was tuned by observing the VP in a right angle triangle prism with a mirror surface positioned at a 45 degree angle. Current density values were calibrated by using a glass-capillary point current source (with an orifice diameter 2 µm) placed 100±5 µm far from the VP. The capillary was filled with 0.05M NaCl. During the calibration, the peak-to-peak vibration amplitude was set equal to 30 µm and the vibration frequencies to 160 Hz in the *horizontal* plane and 99 Hz in the *vertical* plane. For Applicable Electronic equipment any frequency can be chosen in a range of 40-1000 Hz. The used frequency should not influencing vibrations in orthogonal directions and does not coincide with frequencies of power line or its harmonics. Ground and reference electrodes consisted of platinum wires electroplated with Pt black placed either in compartment separated by salt bridge from the VP to avoid possible influence of the inhibitors or in the same compartment to observe inhibitor adsorption on all Pt made electrodes. **Figure 1(a, b)** depicts the experimental set up

used for inspecting of the VP state in presence of corrosion inhibitors. The SVET probe was placed 100 μm far from the current source, which supplied a -60 nA current. The salt bridge was prepared by using a 6cm long plastic tube filled with 0.05 NaCl electrolyte jellified by 3% agar. SVET was re-calibrated before the set of measurements presented in **Figure 6** and **7**. In this case, the peak-to-peak vibration amplitude was 33 μm and the frequencies were 170 Hz in the *horizontal* and 122 Hz in the *vertical* planes. This calibration was used for the measurements of current density in a 0.05 M NaCl solution with addition of MBT where no current flows. SVET measurements shown on **Figure 6** were performed in two different configurations: in the first one, three electrodes (VP, ground and reference electrodes) were placed in the same measurement cell to represent the most typical SVET set up; in the second one, the VP was separated by salt bridge from the reference and the ground electrode to avoid the inhibitor influence on reference and ground electrodes.

Solutions with five different corrosion inhibitors were prepared at neutral pH 6.5-6.7, with 0.05 M NaCl as background electrolyte. The composition and concentration of the used solutions are presented in **Table 1**.

Table 1. List of solutions with inhibitors and respective concentrations.

Inhibitor code	Inhibitor name and concentration
Ce	cerium nitrate, 1mM
DMTD	potassium 2,5-dimercapto-1,3,4-thiadiazolate, 1mM
BTA	benzotriazole, 1mM
8HQ	8-hydroxyquinoline, 1mM
MBT	mercaptobenzothiazole, 0.64 mM (saturated)

OCP and Electrochemical Impedance Spectroscopy.

OCP was measured with a Gamry Reference 600 potentiostat in a three-electrode configuration: Pt wires electroplated with Pt black served as counter and reference electrodes, and the VP as the working electrode. Measurements were performed in two different setups: in the first setup, the VP was separated by salt bridge from ground and reference electrodes; in the second setup, the VP was placed in the same cell compartment with ground and reference electrodes.

Electrochemical impedance spectroscopy measurements were carried out using a Gamry Reference 600 potentiostat in a three-electrode configuration: Pt wire served as counter electrode, Ag/AgCl as reference electrode and a modified version of Pt-Ir wire as working electrode. The modification of

the Pt-Ir wire aimed at increasing the electrochemically active surface area by removing the Parylen C used as probe insulation. The exposed area of the Pt probe was plated with Pt black as follows: the Pt-Ir probe and bare Pt were connected to a 9-volt battery and placed for 10 seconds in the plating solution. The final probe, covered with Pt black (hereafter called "modified VP"), was used only for EIS as working electrode. EIS measurements were repeated twice to ensure the reproducibility. The following procedure was applied before every EIS measurement: first, the Pt-Ir wire was cleaned with ground with emery paper 2400 grit and then Pt black was deposited. Although, the surface area was unknown, the EIS results followed the same trend.

SEM EDX analysies was done at 20kV using Tescan Vega2 SB with EDX spectrometer from iXRF System.

X-ray photoelectron spectroscopy XPS measurements were performed using a KRATOS AXIS Ultra DLD (Kratos Analytical, Manchester, United Kingdom) equipped with a monochromatic Al Kα anode working at 15 kV (225W). For the survey spectra, a pass energy of 160 eV was used for 4 scans each, while for the region spectra the pass energy was 20 eV with 16 scans each. The investigated area was 110 μm in diameter. The evaluation and validation of the data were carried out with the software CASA-XPS version 2.3.18. the spectra calibration was done by adjusting the C1s core signal to 284.5 eV. For deconvolution of the region files, background subtraction (linear or Shirley) was performed before calculation. The samples of interest for XPS was the tip of the VP. The black Pt of the tip was analyzed before immersion and after 30 min immersion in solution containing 8HQ and MBT.

Results and discussion

SVET measurements

The cell configuration depicted in **Figure 1 (a, b)** was used to study the effect of corrosion inhibitors on the VP. **Figure 2** shows the SVET signal in the presence of five different corrosion inhibitors. During the first 20 to 30 min measurements were performed in a pure 0.05 M NaCl aqueous solution. The black line in the plots represents inhibitor-free solution and, beyond this, inhibitor was added as shown by the colored line. Neither the addition of Ce (**Figure 2b**) nor the addition of DMTD (**Figure 2c**) affected the probe signal, showing no effects cause by the inhibitors. In this case, the noise level remained low. However, for the tests with BTA and 8HQ, the noise level of the VP increased. In particular, for the case of 8HQ, the current density revealed also a slight shift of the measured values. In the presence of MBT, the SVET signal became extremely noisy, revealing a very large shift towards negative current densities (**Figure 2f**). This suggested that the presence of 8HQ and MBT in the solution contaminated the VP surface due to the adsorption on the tip of the inhibitor molecules.

The estimated presence of MBT on the SVET probe was confirmed by SEM/EDS investigations.

Figure 3 reveals the surface of the VP after 1 h of immersion in a solution containing 0.64mM MBT. The chloride detected at the probe shaft originated from the chloride containing polymer Parylene C - dielectric isolation used in SVET microprobes. The EDS maps showed Pt as the main element on the VP and S, coming from MBT, located mainly at the tip. This result supports the assumption that MBT molecules are likely to adsorb onto the porous Pt black during the SVET measurements.

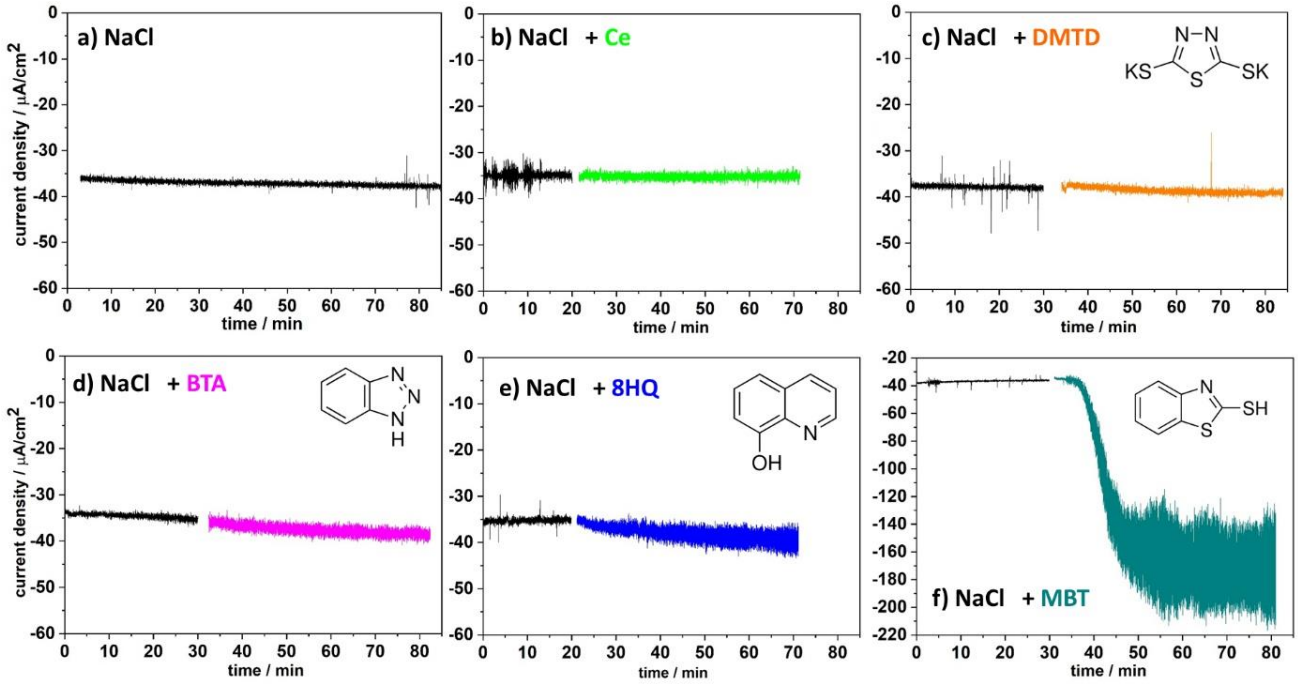

Figure 2. SVET signal, measured in a) pure 0.05 M NaCl aqueous solution including corrosion inhibitors b) Ce, c) DMTD , d) BTA, e) 8HQ and f) MBT.

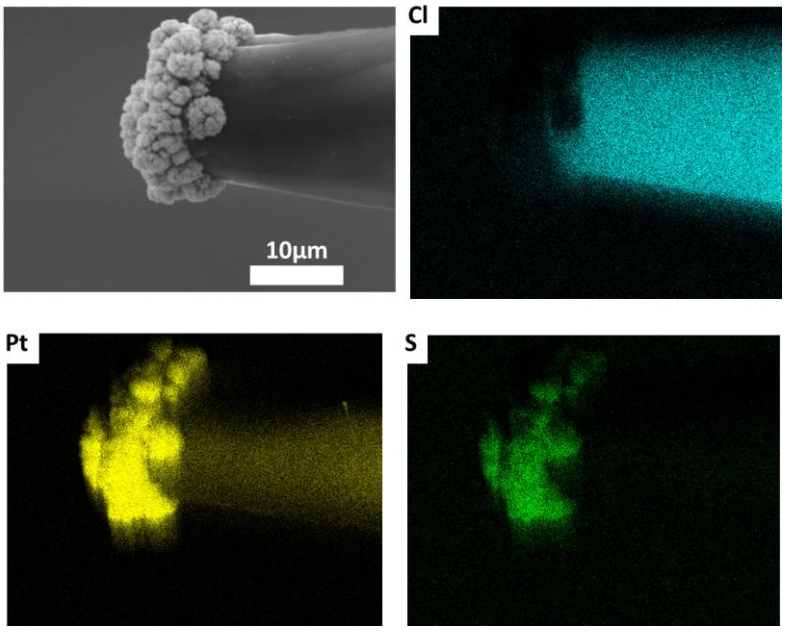

Figure 3. SEM micrograph and EDS elemental mapping of the VP with Pt plated tip after 1h immersion in solution containing 0.64 mM MBT.

EIS measurements

EIS was used to evaluate the electrode-electrolyte interface and to investigate a possible interaction of the inhibitor with the Pt black. **Figure 4** shows the Bode plots of the modified VP (higher surface area of the Pt black) in electrolytes containing five different corrosion inhibitors. The composition of the electrolyte for EIS was the same as for SVET tests shown on **Figure 2**.

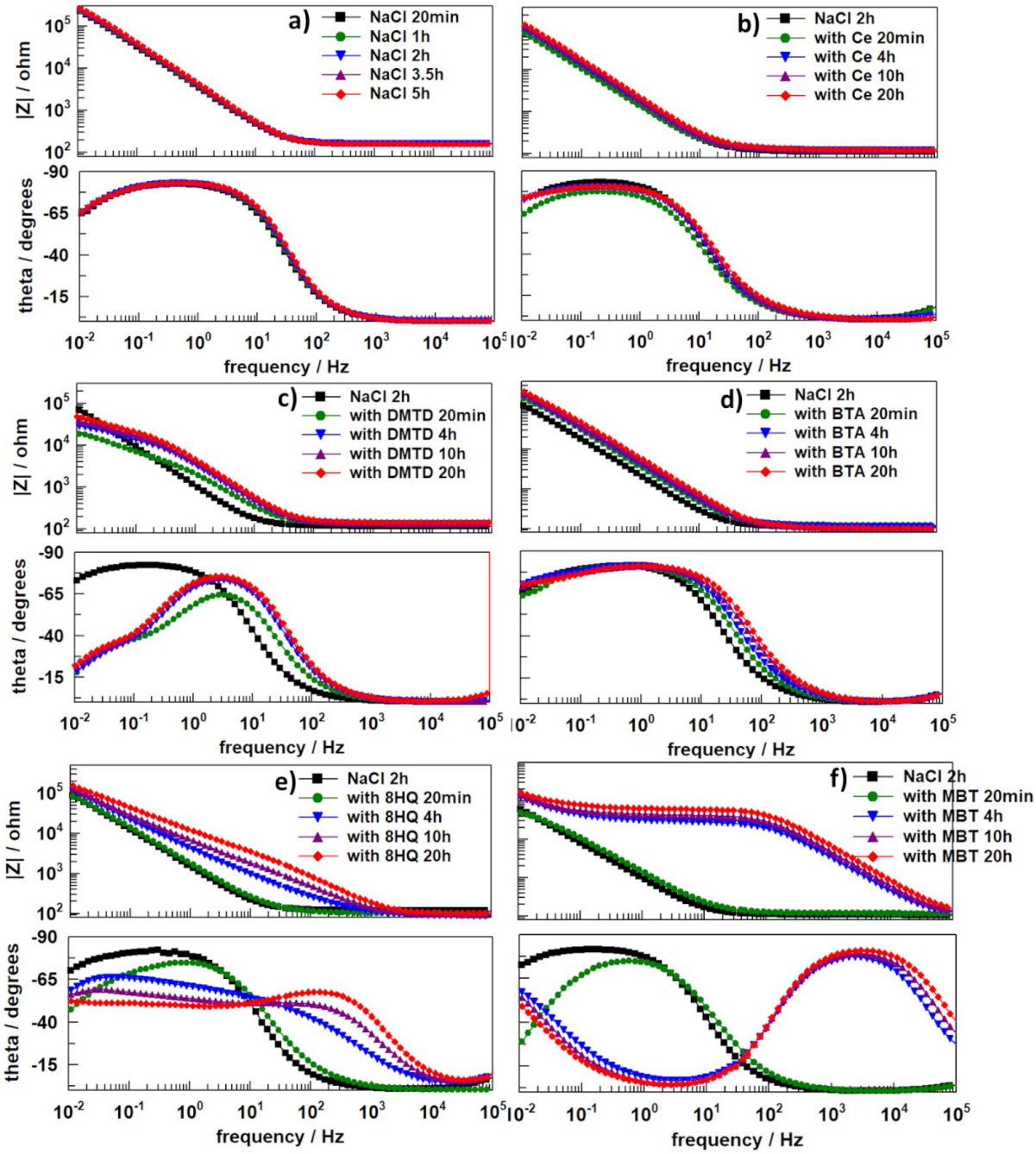

Figure 4. Bode plots for black Pt probe immersed in 0.05 M NaCl (a) and with addition of corrosion inhibitors (b) Ce, (c) DMTD, (d) BTA, (e) 8HQ, (f) MBT.

The impedance units were kept in ohm, since the surface area of the modified VP was unknown.

At first, the impedance of the VP in pure NaCl was measured. The impedance spectra in NaCl reveals one time constant which is typical for the metal-electrolyte interface (**Figure 4a**) [43]. For Ce and BTA as inhibitors (**Figure 4b and 4d**) EIS spectra clearly demonstrates that no changes of the impedance values occurred during immersion. Although BTA exhibited one time constant, it shifted towards higher frequencies with increasing immersion time, suggesting a slight capacitance decrease. The EIS results for the DMTD, 8HQ and MBT displayed two time constants. The high frequency time constant is related to the thin layer of inhibitors adsorbed on the surface. For the EIS spectra of the DMTD, a reduction of the capacitance was observed during the first 4h of immersion. The subsequent results did not reveal changes by time. A different trend was observed for 8HQ and MBT. Adding 8HQ slightly changed the impedance of the probe at an early stage. However, during the experiment the high frequency time constant became well evident: this effect might be the consequence of a dynamical growth of the adsorbed layer on the Pt surface. As the immersion time elapsed (4h, 10h, 20h), the low frequency region revealed a phase angel close to 45°. This behavior might be related with the diffusion-controlled process. The EIS spectra of MBT showed the presence of an adsorbed layer of inhibitor since the first minutes after addition of MBT, which becomes more evident as the time passes. The impedance behavior suggests that the mechanism of adsorption for 8HQ and MBT are different, as 8HQ, DMTD and MBT are heterocyclic compounds with different interaction kinetics to the metal. Different formation mechanisms of very thin adsorbed protective layers on the surface of copper [44, 45] and aluminum [46] have already been observed. The complexation reactions of MBT-derivatives with Pt, Ir and Pd were also expected [47].

The presence of an adsorbed layer on the VP is able to affect the signal and may cause false results during the SVET measurements. Both SVET and EIS results suggest that the sensitivity of the VP is slightly affected by use of DMTD and BTA, whereas the influence of 8HQ and MBT is significant due to formation of adsorbed layers on the surface of the electrode leading to decrease of the VP capacitance.

XPS measurements

The formation of an adsorbed layer of 8HQ and MBT at the surface of black Pt was investigated by X-ray photoelectron spectroscopy. These two inhibitors were selected because of their strong interaction with the probe surface. To identify the changes on the VP surface with XPS, the measurements for black Pt before immersion and after 30 min immersion in 1mM 8HQ solution (**Figure 5a**) and 0.64 mM MBT (**Figure 5b, c**) were performed.

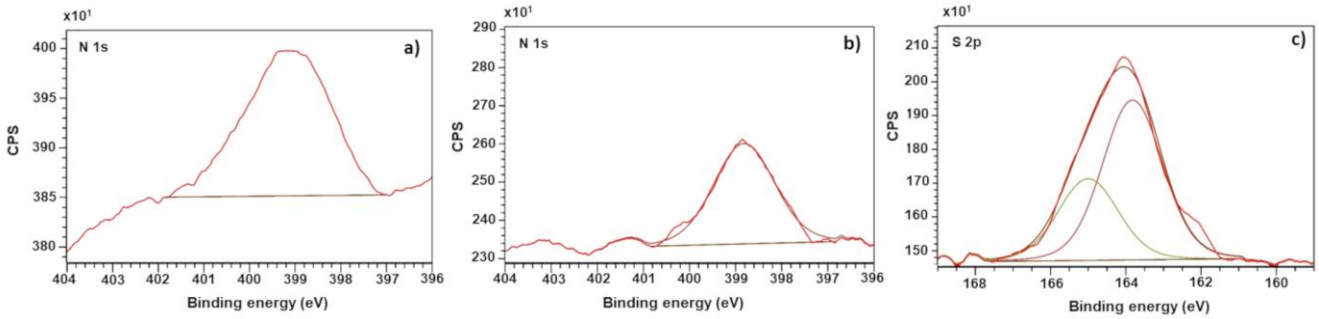

Figure 5. XPS deconvoluted core regions for (a) N 1s for the VP after 8HQ, and (b) N1s and (c) S 2p for the VP after MBT.

The results suggest the N1s XPS pick after immersion in 8HQ solution. Deconvoluted spectra of the N1s envelope are shown on **Figure 5a**. The N1s peak has a binding energy of 399.2 eV and can be assigned to N in aromatic rings [48]. The origin of nitrogen is related to the adsorbed 8HQ at the VP surface due to its ability to form chelates with diverse metals [13, 49, 50].

After exposure of the VP to the solutions with MBT, the nitrogen and sulphur picks were detected. **Figure 5b and c** presents the deconvolution of the N1s and S 2p picks. The N1s peak was placed at 398.8 eV and corresponds to nitrogen in aromatic ring system [48]. The S2p pick was deconvoluted to the corresponding spin-orbit doublet of $S2p_{3/2}$ and $S2p_{1/2}$ states (ΔeV=1.16eV ratio 0.511). The binding energy of 163.8 eV typical for thiol-containing compounds [48]. These results qualitatively confirm the adsorption of MBT on the surface of the black Pt probe.

What is the reason of shift to a negative current density in presence of MBT?

In order to find the reason of the current density increase towards negative values measured near point current source (**Figure 2f**), an additional set of experiments was performed without current flowing through the cell. **Figure 6** shows the SVET results measured in two different setups, when vibrating and reference electrodes were placed in the same cell, and when vibrating and reference electrodes were separated by salt bridge. In the later set-up the MBT was in contact only with the VP. The electric field should be zero when the solution is at rest. However, **Figure 6** shows the apparent negative current density, even when there are no current sources in the cell. The origin of this signal might be the notable background voltage gradient emerged between vibrating and reference electrodes in presence of MBT. In order to confirm this assumption, the difference of electrical potential between vibrating and reference electrode was assessed in two different setups and results are shown on **Figure 6**. When MBT was added into the electrolyte, it adsorbed on the tip of the VP and on the reference electrode when the measurements were done in one compartment of the cell. This process led to changes of the electrode surface and creates a difference of potential between vibrating and reference electrodes, which is taken by SVET device as a signal. The measured current density represents the voltage gradient at the measuring point. Under normal conditions, the

background voltage gradient is not significant. However, in presence of MBT, the voltage gradient presented sharp changes which are transformed to a current density signal [32]. Thus, in MBT solution with no significant currents, the voltage field is defined by the voltage gradient between vibrating and reference electrode. The negative sign of the current density might be explained according to **eq. 1**. The solution conductivity k remains constant as well as Δr between two measuring points, thereby the value and sign of i depends on the potential difference ΔV measured between two points. Stable potential is observed during first 12 min in non-inhibitor electrolyte. ΔV is increasing with time (**Figure 6**), leading to high negative values of current density when MBT is added.

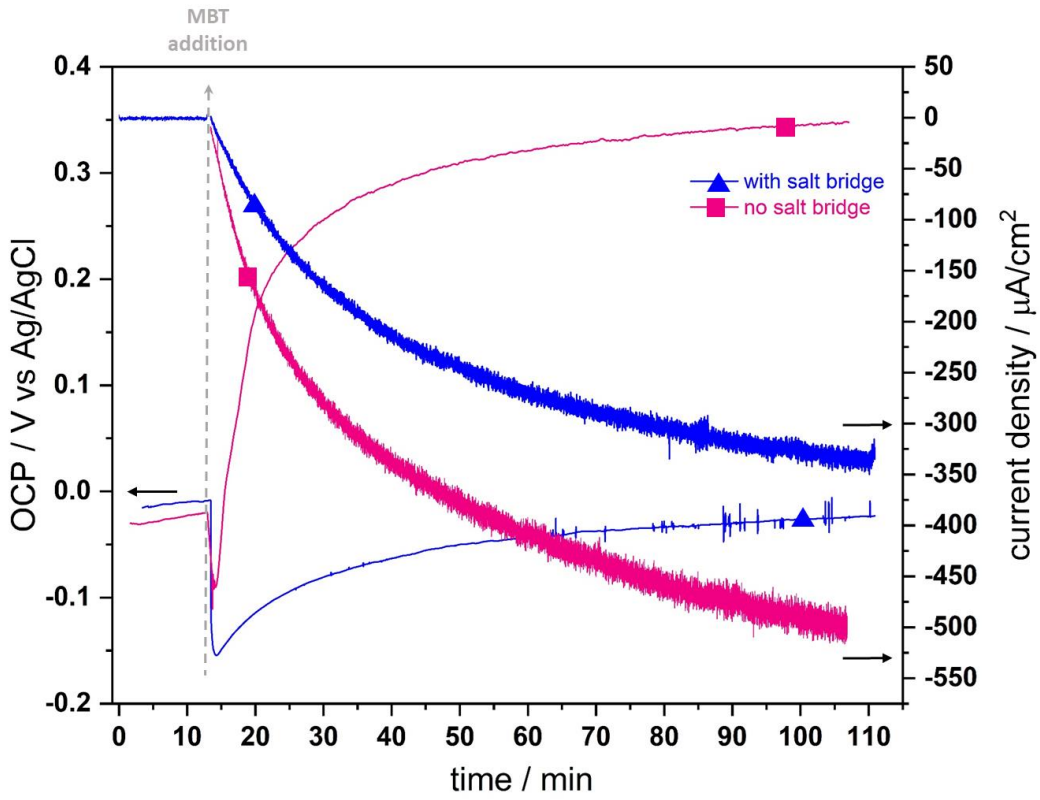

Figure 6. Comparison of SVET signal (no flowing current) with OCP of the VP in 0.05M NaCl with addition of MBT in different cell configuration: (▲) the VP is separated by salt bridge from ground and reference electrodes, (■) the VP is placed in the same cell compartment with ground and reference electrodes. In latter case, MBT gradually adsorbs on all three Pt made probes: VP, reference and ground.

From the OCP results, it appears that the difference in potential between the vibrating and the reference electrode is more than 300 mV when the measurements were done in the same cell. The same difference is approx. 150 mV when only the VP was in contact with MBT (**Figure 6**). This difference could explain the more rapid changes in the current density when both electrodes were immersed in the MBT solution. When both electrodes were exposed to MBT, the inhibitor adsorbs on platinized surface changing its properties and producing a more significant voltage drop. However, due to the significant difference in the surface area of the VP and reference electrodes, adsorption

kinetics were different.

Summarizing, the presence of an inhibitor can differently affect the SVET measurements and be the cause of a high signal noise and false current densities. The increased signal noise is related to the decrease of the VP capacitance. The false current signal is related to a potential drift between VP and reference electrode.

SVET measurement in solution with different concentration of inhibitor

MBT is a common corrosion inhibitor widely studied to protect copper, AA2024 and other metals. From the above discussed results, the biggest impact of the inhibitor adsorption on the VP was observed when MBT was present in the electrolyte. Thus, a key question arises: *which experimental conditions enable valid SVET measurements in presence of MBT in the electrolyte*? One of the apparent answers is that a low MBT concentration might not affect the VP conditions. The following experiment was carried out to investigate the condition of the VP and its sensitivity depending on the MBT concentration. First, the signal of the VP was assessed in the MBT solution where no current flows. To simulate the real SVET measuring conditions, the reference and ground electrodes were placed in the same cell. Three different MBT concentrations were tested; 0.64, 0.064 and 0.0027 mM. The behavior of the system at alkaline pH was also verified, because an alkaline environment is characteristic for the areas of cathodic activity during corrosion processes. MBT exists in different forms, in aqueous solutions, depending on the pH of the electrolyte and as follows from its stability constant pKa=6.93 [51].

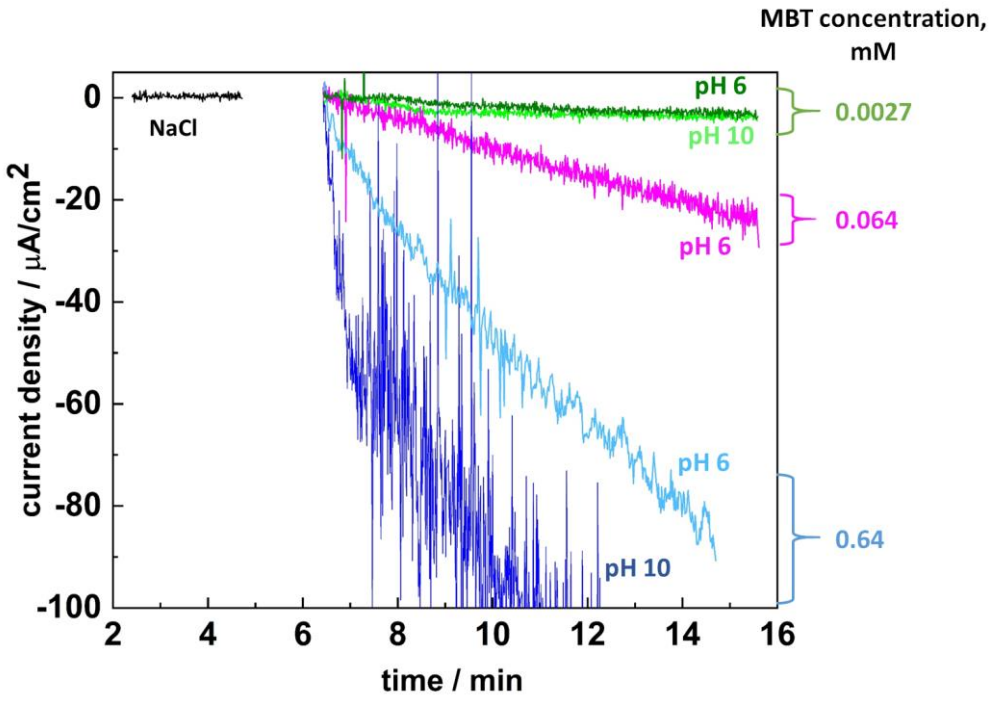

Figure 7. Variation of the SVET signal without current source in 0.05 M NaCl with addition of MBT at different concentrations and different pH.

Figure 7 shows the evolution of SVET signal for different conditions: no change in the probe performance was detected for low concentration (0.0027 mM). The pH alkalinization held the probe signal close to 0 with a low level of noise. Comparing the probe performance at a higher MBT concentration (0.064.mM), it is evident that the noise of the signal increased with a remarkable drift of the current density. A further increase of the MBT concentration lead to a large change in the current density, which was detected at the very beginning of the immersion. The increase of pH also led to an even stronger noise on the SVET signal, together with more rapid changes in the current density. The different behavior observed at pH 6 and 10 could be explained by the presence of different forms of MBT. At neutral pH, mercaptobenzohiazole is present mainly in the undissociated form MBT-SH, and at alkaline pH it is present mostly as negatively charged MBT-S^-. The interaction with Pt is more significant with the deprotonated form of MBT.

SVET measurements in presence of organic and inorganic inhibitors might become complicated by the adsorption of the inhibitor on the highly developed surface of Pt black constituting the sensitive part of SVET probe. This effect decreases as the inhibitor concentration decreases. These phenomena are not expected for the inhibitor-loaded coatings. There, the decrease of local current density is achieved by the release of a small amount of inhibitor into the confined micro-volume around the defect: the inhibitor interacts locally with a substrate or a coating suppressing the corrosion. The effect of each new inhibitor on the readings of the SVET probe needs therefore to be verified to prevent false results of SVET measurements.

Conclusions

This work studied the effect of different corrosion inhibitors on the condition and the response of the VP covered with a Pt black typically used for measurements of local current densities by SVET. Five corrosion inhibitors were tested: cerium nitrate (Ce), 8-hydroxyquinoline (8HQ), 1,3,4-thiadiazole- 2,5 -dithiol dipotassium salt (DMTD), benzotriazole (BTA) and mercaptobenzothiazole (MBT). SVET, EIS and XPS confirmed that 8HQ and MBT were adsorbed on the surface of the probe. Cerium nitrate was found not to influence the readings of the Pt probe. BTA and DMTD slightly decreased the capacitance of the probe and made the signal to noise ratio lower. 8HQ and especially MBT dramatically increased the noise of the SVET measurements due to the inhibitor adsorption on the probe. Moreover, MBT affected the values of the current density. The significant shift towards a negative current density was a result of the potential drift between vibrating and reference electrodes due to different adsorption kinetic of MBT.

Naturally, if the signal of the probe drifts or possess very high noise, important precautions must be taken, such as: decreasing the concentration of inhibitor, or cleaning the probe with further replating with black Pt before every measurement.

SVET can be safely used to study the efficiency of different inhibitors in coatings with defects, for example to evaluate the self-healing effect of polymeric anti-corrosion coatings, since in this case the concentration of inhibitor released from the coating into the defect is typically low and confined in the defect volume. The concentration of the inhibitor that is released from the coating into the solution should be taken into consideration, and in general should be low, for a reliable interpretation of the SVET measurements. However, the adsorption of any corrosion inhibitor on vibrating probe is hard to predict. This phenomena needs to be verified individually prior to studying inhibitor efficiency by SVET. The effect of inhibitor adsorption is not exclusively SVET problem but may affect other localized measurements like SECM, LEIS, and the like where Pt probes are used.

Acknowledgments

D. Snihirova acknowledges the Humboldt foundation for her Postdoctoral grant and Dr. A. Bastos and Dr. M.Taryba for scientific discussions. Additionally, Mr. U. Burmester and Mr. V. Heitmann are acknowledged for the technical support. M.F. Montemor thanks Fundação para a Ciência e a Tecnologia (FCT, Portugal) for the financial support under the project UID/QUI/00100/2019.

Data availability

The raw/processed data required to reproduce these findings cannot be shared at this time as the data also forms part of an ongoing study.

References

[1] L.F. Jaffe, R. Nuccitelli, AN ULTRASENSITIVE VIBRATING PROBE FOR MEASURING STEADY EXTRACELLULAR CURRENTS, The Journal of Cell Biology, 63 (1974) 614-628.
[2] R. Nuccitelli, A two-dimensional vibrating probe with a computerized graphics display., in: R. Nuccitelli, A. Liss (Eds.) Ionic Currents in Development - Progress in Clinical and Biological Research, New York, 1986, pp. 13-20.
[3] C. Scheffey, Two approaches to construction of vibrating probes for electrical current measurement in solution, Review of Scientific Instruments, 59 (1988) 787-792.
[4] B. Reid, R. Nuccitelli, M. Zhao, Non-invasive measurement of bioelectric currents with a vibrating probe, Nature Protocols, 2 (2007) 661.
[5] C. Scheffey, Pitfalls of the vibrating probe technique, and what to do about them, in: R. Nuccitelli, A. Liss (Eds.) Ionic Currents in Development - Progress in Clinical and Biological Research, New York, 1986, pp. 3-12.
[6] H.S. Isaacs, Applications of current measurement over corroding metallic surfaces, in: R. Nuccitelli, A. Liss (Eds.) Ionic Currents in Development - Progress in Clinical and Biological Research, New York, 1986, pp. 37-44.
[7] H.S. Isaacs, Y. Ishikawa, Current and Potential Transients during Localized Corrosion of Stainless Steel, J Electrochem Soc, 132 (1985) 1288-1293.
[8] H.S. Isaacs, Limitations of In Situ Current Density Mapping for Vibrating Electrodes Close to Metal Surfaces, CORROSION, 46 (1990) 677-679.
[9] H.S. Isaacs, The Effect of Height on the Current Distribution Measured with a Vibrating Electrode Probe, J Electrochem Soc, 138 (1991) 722-728.
[10] S. Kallip, A.C. Bastos, M.L. Zheludkevich, M.G.S. Ferreira, A multi-electrode cell for high-throughput SVET

screening of corrosion inhibitors, Corros Sci, 52 (2010) 3146-3149.
[11] S. Kallip, A.C. Bastos, K.A. Yasakau, M.L. Zheludkevich, M.G.S. Ferreira, Synergistic corrosion inhibition on galvanically coupled metallic materials, Electrochem Commun, 20 (2012) 101-104.
[12] G. Williams, A.J. Coleman, H.N. McMurray, Inhibition of Aluminium Alloy AA2024-T3 pitting corrosion by copper complexing compounds, Electrochim Acta, 55 (2010) 5947-5958.
[13] D. Snihirova, M. Taryba, S.V. Lamaka, M.F. Montemor, Corrosion inhibition synergies on a model Al-Cu-Mg sample studied by localized scanning electrochemical techniques, Corros Sci, 112 (2016) 408-417.
[14] L.B. Coelho, M.G. Olivier, The inhibition efficiency of different species on AA2024/graphite galvanic coupling models depicted by SVET, Corros Sci, 136 (2018) 292-303.
[15] T. Hu, H. Shi, D. Hou, T. Wei, S. Fan, F. Liu, E.-H. Han, A localized approach to study corrosion inhibition of intermetallic phases of AA 2024-T3 by cerium malate, Applied Surface Science, 467-468 (2019) 1011-1032.
[16] A.C. Bastos, M.G. Ferreira, A.M. Simões, Corrosion inhibition by chromate and phosphate extracts for iron substrates studied by EIS and SVET, Corros Sci, 48 (2006) 1500-1512.
[17] M.J. Franklin, D.C. White, H.S. Isaacs, A study of carbon steel corrosion inhibition by phosphate ions and by an organic buffer using a scanning vibrating electrode, Corros Sci, 33 (1992) 251-260.
[18] A.M. Simões, J. Torres, R. Picciochi, J.C.S. Fernandes, Corrosion inhibition at galvanized steel cut edges by phosphate pigments, Electrochim Acta, 54 (2009) 3857-3865.
[19] C.F. Glover, G. Williams, Inhibition of Localized Corrosion of Hot Dip Galvanized Steel by Phenylphosphonic Acid, J Electrochem Soc, 164 (2017) C407-C417.
[20] G. Williams, R. Grace, R.M. Woods, Inhibition of the Localized Corrosion of Mg Alloy AZ31 in Chloride Containing Electrolyte, CORROSION, 71 (2015) 184-198.
[21] F. Cotting, I.V. Aoki, Smart protection provided by epoxy clear coating doped with polystyrene microcapsules containing silanol and Ce (III) ions as corrosion inhibitors, Surface and Coatings Technology, 303 (2016) 310-318.
[22] M.F. Montemor, D.V. Snihirova, M.G. Taryba, S.V. Lamaka, I.A. Kartsonakis, A.C. Balaskas, G.C. Kordas, J. Tedim, A. Kuznetsova, M.L. Zheludkevich, M.G.S. Ferreira, Evaluation of self-healing ability in protective coatings modified with combinations of layered double hydroxides and cerium molibdate nanocontainers filled with corrosion inhibitors, Electrochim Acta, 60 (2012) 31-40.
[23] M. Plawecka, D. Snihirova, B. Martins, K. Szczepanowicz, P. Warszynski, M.F. Montemor, Self healing ability of inhibitor-containing nanocapsules loaded in epoxy coatings applied on aluminium 5083 and galvanneal substrates, Electrochim Acta, 140 (2014) 282-293.
[24] N. Pirhady Tavandashti, M. Ghorbani, A. Shojaei, J.M.C. Mol, H. Terryn, K. Baert, Y. Gonzalez-Garcia, Inhibitor-loaded conducting polymer capsules for active corrosion protection of coating defects, Corros Sci, 112 (2016) 138-149.
[25] T. Hu, H. Shi, S. Fan, F. Liu, E.-H. Han, Cerium tartrate as a pigment in epoxy coatings for corrosion protection of AA 2024-T3, Prog Org Coat, 105 (2017) 123-131.
[26] F. Maia, K.A. Yasakau, J. Carneiro, S. Kallip, J. Tedim, T. Henriques, A. Cabral, J. Venâncio, M.L. Zheludkevich, M.G.S. Ferreira, Corrosion protection of AA2024 by sol–gel coatings modified with MBT-loaded polyurea microcapsules, Chem. Eng. J., 283 (2016) 1108-1117.
[27] M. Taryba, S.V. Lamaka, D. Snihirova, M.G.S. Ferreira, M.F. Montemor, W.K. Wijting, S. Toews, G. Grundmeier, The combined use of scanning vibrating electrode technique and micro-potentiometry to assess the self-repair processes in defects on “smart” coatings applied to galvanized steel, Electrochim Acta, 56 (2011) 4475-4488.
[28] D. Snihirova, L. Liphardt, G. Grundmeier, F. Montemor, Electrochemical study of the corrosion inhibition ability of “smart” coatings applied on AA2024, J. Solid State Electrochem., (2013) 1-10.
[29] I.A. Kartsonakis, E. Athanasopoulou, D. Snihirova, B. Martins, M.A. Koklioti, M.F. Montemor, G. Kordas, C.A. Charitidis, Multifunctional epoxy coatings combining a mixture of traps and inhibitor loaded nanocontainers for corrosion protection of AA2024-T3, Corros Sci, 85 (2014) 147-159.
[30] V. Upadhyay, D. Battocchi, Localized electrochemical characterization of organic coatings: A brief review, Prog

Org Coat, 99 (2016) 365-377.
[31] A.C. Bastos, M.C. Quevedo, M.G.S. Ferreira, The influence of vibration and probe movement on SVET measurements, Corros Sci, 92 (2015) 309-314.
[32] C. Scheffey, Tutorial: Electric fields and the vibrating probe, for the uninitiated, in: R. Nuccitelli (Ed.) Ionic currents in development, Alan R. Liss, INC, New york, 1986, pp. xxv-xxxvii.
[33] Applicable Electronics. Scanning vibrating electrode technique (SVET) for electrophysiology. System manual., 2014.
[34] M.L. Zheludkevich, K.A. Yasakau, A.C. Bastos, O.V. Karavai, M.G.S. Ferreira, On the application of electrochemical impedance spectroscopy to study the self-healing properties of protective coatings, Electrochem Commun, 9 (2007) 2622-2628.
[35] S.J. García, H.R. Fischer, P.A. White, J. Mardel, Y. González-García, J.M.C. Mol, A.E. Hughes, Self-healing anticorrosive organic coating based on an encapsulated water reactive silyl ester: Synthesis and proof of concept, Prog Org Coat, 70 (2011) 142-149.
[36] A.C. Bastos, M.C. Quevedo, O.V. Karavai, M.G.S. Ferreira, Review—On the Application of the Scanning Vibrating Electrode Technique (SVET) to Corrosion Research, J Electrochem Soc, 164 (2017) C973-C990.
[37] Y. Gonzalez-Garcia, S.J. Garcia, J.M.C. Mol, Electrochemical Techniques for the Study of Self Healing Coatings, in: E.A. Hughes, M.C.J. Mol, L.M. Zheludkevich, G.R. Buchheit (Eds.) Active Protective Coatings: New-Generation Coatings for Metals, Springer Netherlands, Dordrecht, 2016, pp. 203-240.
[38] R. Scott Lillard, Scanning Electrode Techniques for Investigating Near-Surface Solution Current Densities, in: P. Marcus, F. Mansfeld (Eds.) Analytical Methods in Corrosion Science and Engineering, CRC Press, Boca Raton, 2006.
[39] A.C. Bouali, A.C. Bastos, S.V. Lamaka, M. Serdechnova, M.G.S. Ferreira, L.M. Zheludkevich, Evaporation of Electrolyte During SVET Measurements: The Scale of the Problem and the Solutions, Electroanalysis, accepted (2019).
[40] H.N. McMurray, D. Williams, D.A. Worsley, Artifacts Induced by Large-Amplitude Probe Vibrations in Localized Corrosion Measured by SVET, J Electrochem Soc, 150 (2003) B567-B573.
[41] A.S. Demeter, O. Dolgikh, A.C. Bastos, D. Deconinck, S. Lamaka, V. Topa, J. Deconinck, Multi-ion transport and reaction model used to improve the understanding of local current density measurements in presence of concentration gradients around a point current source, Electrochim Acta, 127 (2014) 45-52.
[42] I. Recloux, Y. Gonzalez-Garcia, M.E. Druart, F. Khelifa, P. Dubois, J.M.C. Mol, M.G. Olivier, Active and passive protection of AA2024-T3 by a hybrid inhibitor doped mesoporous sol–gel and top coating system, Surface and Coatings Technology, 303 (2016) 352-361.
[43] A. Norlin, J. Pan, C. Leygraf, Investigation of interfacial capacitance of Pt, Ti and TiN coated electrodes by electrochemical impedance spectroscopy, Biomol. Eng, 19 (2002) 67-71.
[44] L.P. Kazansky, Y.E. Pronin, I.A. Arkhipushkin, XPS study of adsorption of 2-mercaptobenzothiazole on a brass surface, Corros Sci, 89 (2014) 21-29.
[45] Y. Kuznetsov, L.P. Kazansky, Physicochemical aspects of metal protection by azoles as corrosion inhibitors Usp. Khim., 77 (2008) 227-241.
[46] S.V. Lamaka, M.L. Zheludkevich, K.A. Yasakau, M.F. Montemor, M.G.S. Ferreira, High effective organic corrosion inhibitors for 2024 aluminium alloy, Electrochim Acta, 52 (2007) 7231-7247.
[47] Q. Pu, Z. Su, Z. Hu, X. Chang, M. Yang, 2-Mercaptobenzothiazole-bonded silica gel as selective adsorbent for preconcentration of gold, platinum and palladium prior to their simultaneous inductively coupled plasma optical emission spectrometric determination, J. Anal. At. Spectrom., 13 (1998) 249-253.
[48] A.N. Naumkin, A. Kraut-Vass, S.W. Gaarenstroom, C.J. Powell, NIST X-ray Photoelectron Spectroscopy Database, in: N.I.o.S.a. Technology (Ed.), Gaithersburg MD, 2012.
[49] H. Gerengi, M. Mielniczek, G. Gece, M.M. Solomon, Experimental and Quantum Chemical Evaluation of 8-Hydroxyquinoline as a Corrosion Inhibitor for Copper in 0.1 M HCl, Industrial & Engineering Chemistry Research, 55 (2016) 9614-9624.

[50] S.V. Lamaka, B. Vaghefinazari, D. Mei, R.P. Petrauskas, D. Höche, M.L. Zheludkevich, Comprehensive screening of Mg corrosion inhibitors, Corros Sci, 128 (2017) 224-240.
[51] A. Martell, R. Smith, Critical stability contants. Other organic ligands, 1977.